Using normal modes to calculate and optimize thermal conductivity in functionalized macromolecules

Abdellah Ait Moussa* and Kieran Mullen
Homer L. Dodge Department of Physics and Astronomy, The University of Oklahoma, 440 West Brooks Street, Norman, Oklahoma 73019-0225, USA
(Received 4 January 2011; published 16 May 2011)

The quest for high thermal conductivity materials has led to nanocomposites incorporating macromolecular materials with excellent thermal conductivity, such as carbon nanotubes and graphene nanoribbons, in a matrix of poorer thermal conductivity. To minimize the interface thermal resistance the stiff, incorporated materials can be chemically functionalized with various side chains. We report here an efficient theoretical method using normal modes to calculate the thermal conductivity of such systems and show how the participation ratio of these modes can be used to evaluate different choices for functionalization. We use this method to examine how effective different alkane chains improve the heat flux through a graphene nanosheet.

DOI: 10.1103/PhysRevE.83.056708 PACS number(s): 02.60.−x, 65.80.Ck

I. INTRODUCTION

The thermal conductivity of single wall carbon nanotubes (CNTs) at room temperature is about 6000 W/mK and that of multiwall carbon nanotubes is about 3000 W/mK [1–3]. Graphene also displays a number of remarkable properties including extremely high electron mobility (up to $\sim 2 \times 10^5$ cm^2/Vs [4,5]), and extremely high thermal conductivity (ranging from $(4.84 \pm 0.44) \times 10^3$ to $(5.30 \pm 0.48) \times 10^3$ $Wm^{-1}K^{-1}$ [6]). The thermal conductivity of graphene and few-layer graphene depends strongly on the size of the graphene flakes [7] and the thickness of the few-layer graphene [8]. The outstanding thermal performance of these materials suggests their use in thermal management applications in electronics and optoelectronics [9–12].

However, the incorporation of CNTs and graphene into polymers has not produced the high thermal conductivity composites because of the constituents' interface thermal resistance. "Kapitza resistance" occurs at the boundary of two dissimilar materials [13,14] and produces a temperature drop across the interface that is proportional to the heat flux. The effect is large when the two materials have a large difference in elasticity so that there is only a weak coupling of phonon modes at the interface. If this resistance could be minimized then polymer composites could be used in radiators and other heat exchangers replacing heavier, costlier metallic components.

To this end, in the graphene system two strategies have been proposed. The first is based on the fabrication of graphene strips with reduced lateral size [known as graphene nanoribbons (GNRs)] [15]. GNRs with width(s) from several tens of nanometers down to 2 nm have been fabricated either by plasma etching [16] or by means of chemical treatment of graphite [17]. Alternatively, chemical functionalization of graphene-based materials is a promising strategy and does not require aggressive ribbon width reduction. Nevertheless this method may induce severe disruption of the otherwise good conducting properties of graphene. Optimizing the thermal conduction to the graphene appears then to be a major challenge, and constructing models to simulate the heat conduction to the graphene tend to be helpful.

In this paper we introduce a new technique to calculating thermal conductivity of functionalized molecules in general and use graphene nanosheets as a case study. We show by linearizing the interatomic interactions, and by numerically calculating the normal modes, that the total heat flux, throughout the functionalized macromolecule is a function of the temperature difference of the hot and cold baths. Even more interestingly, we show that we can control the heat transport throughout the system by varying the functionalized chains.

It may be objected that linearizing interactions dramatically changes the dynamics of the system. However, we are interested in determining the major bottlenecks to thermal conductivity at the interface and these are present even in the linear approximation. Nonlinear corrections may alter the magnitude of our results, but not the essential principles for optimization.

This paper is divided into three major parts. In the first, we introduce the analytical technique used to solve for the thermal heat flux of a system of interacting particles the first and last of which are in contact with thermal heat baths. Next, we numerically apply this technique to two systems: an idealized one-dimensional chain and a more realistic functionalized graphene nanosheet. We further analyze the effect of changing the length of the chains on the overall conduction of heat throughout the functionalized graphene and we verify the validity of these results by calculating the participation ratio. In the final section we conclude with a summary and discussion.

II. THE ANALYTICAL TECHNIQUE

A. Site displacement

In this section, we shall develop the general Langevin formalism that we apply to a specific system in Sec. III. We shall present this general case first and then indicate briefly how the results will simplify for our special cases.

Consider a system made of N particles connected by springs. We will apply a driving random force to the first

*Abdellah.Ait.Moussa-1@ou.edu

and last particles. Each particle obeys the equation of motion:

$$m_i \ddot{X}_i = -\sum_j K_{ij} X_j + [\gamma_i \dot{X}_i + F_i(t)](\delta_{i,1} + \delta_{i,N}), \quad (1)$$

where m_i, X_i, respectively, are the mass and displacement of particle i, K_{ij} is the spring constant between particles i and j, γ_i the damping force given by Stokes's law, $F_i(t)$ is the Langevin force on particle i, the overhead dot refers to time derivative, and δ_{ij} is the Kronecker delta function restricting the driving and damping to the first and last particles.

We can write the set of N coupled differential equations as

$$\widetilde{M}\ddot{\vec{X}} + \widetilde{\Gamma}\dot{\vec{X}} + \widetilde{K}\vec{X} = \vec{F}(t), \quad (2)$$

where $\widetilde{M}$, $\widetilde{\Gamma}$, $\widetilde{K}$ are, respectively, the mass, damping, and spring constant matrices and $\vec{F}(t)$ is the random Langevin force vector.

The statistics of the Langevin sources [18] are defined by

$$\langle F_i(t)\rangle = 0, \quad (3)$$

$$\langle F_i(t_1)F_j(t_2)\rangle = 2\gamma_i k_B T_i \delta_{ij}\delta(t_1 - t_2), \quad (4)$$

where T_i is the temperature of the source i, k_B is the Boltzman constant, and $\langle\,\rangle$ stands for temporal average.

Consider the homogeneous form of Eq. (2),

$$\widetilde{M}\ddot{\vec{X}} + \widetilde{\Gamma}\dot{\vec{X}} + \widetilde{K}\vec{X} = 0. \quad (5)$$

We search for a solution to Eq. (5) of the form $\vec{X} = \vec{a}e^{\lambda t}$, where $\vec{a}$ is independent of the time t. Plugging this solution in Eq. (5) gives

$$\widetilde{M}\lambda^2\vec{a} + \lambda\widetilde{\Gamma}\vec{a} + \widetilde{K}\vec{a} = 0. \quad (6)$$

This is a quadratic eigenvalue problem for λ. To solve this eigenvalue problem we introduce a second set of coefficients,

$$\vec{b} = \lambda\vec{a}, \quad (7)$$

and Eq. (6) becomes

$$\lambda\widetilde{M}\vec{b} + \widetilde{\Gamma}\vec{b} + \widetilde{K}\vec{a} = 0, \quad (8)$$

producing an eigenvalue equation of the form,

$$\begin{pmatrix} \widetilde{0} & \widetilde{1} \\ \widetilde{K} & \widetilde{\Gamma} \end{pmatrix}\begin{pmatrix} \vec{a} \\ \vec{b} \end{pmatrix} = \lambda\begin{pmatrix} \widetilde{1} & \widetilde{0} \\ \widetilde{0} & -\widetilde{M} \end{pmatrix}\begin{pmatrix} \vec{a} \\ \vec{b} \end{pmatrix}, \quad (9)$$

where $\widetilde{1}$ is the unity matrix. Thus we see that *even in the presence of dissipation,* we can find normal, uncoupled modes for the system.

In general we generate complex eigenvalues λ_k and complex eigenvectors $\vec{a}_k$. However, if λ_k and $\vec{a}_k$ are solutions to the eigenvalue problem then their complex conjugates λ_k^* and $\vec{a}_k^*$ are solutions as well. Let

$$\lambda_k = -\eta_k + i\omega_k, \quad (10)$$

and

$$\vec{a}_k = \vec{u}_k + i\vec{v}_k, \quad (11)$$

then

$$\vec{a}_k e^{\lambda_k t} = (\vec{u}_k + i\vec{v}_k)e^{-\eta_k t + i\omega_k t} \quad (12)$$

is a solution to the homogenous equation of motion [Eq. (5)] and so is

$$\vec{a}_k^* e^{\lambda_k^* t} = (\vec{u}_k - i\vec{v}_k)e^{-\eta_k t - i\omega_k t}. \quad (13)$$

Thus we can define the real solutions $\chi_k^{(1)}(t)$ and $\chi_k^{(2)}(t)$, where

$$\chi_k^{(1)}(t) = e^{-\eta_k t}[\vec{u}_k \cos(\omega_k t) - \vec{v}_k \sin(\omega_k t)], \quad (14)$$

$$\chi_k^{(2)}(t) = e^{-\eta_k t}[\vec{u}_k \sin(\omega_k t) + \vec{v}_k \cos(\omega_k t)], \quad (15)$$

and from that the general solution to the homogenous problem is

$$\vec{\chi}(t)^{\text{hom}} = \sum_k B_k^{(1)}\chi_k^{(1)}(t) + B_k^{(2)}\chi_k^{(2)}(t), \quad (16)$$

where $B_k^{(1)}$ and $B_k^{(2)}$ are constants that depend on the boundary conditions.

The solution to the driven problem of Eq. (2) is

$$\vec{\chi}(t) = \vec{\chi}(t)^{\text{hom}} + \int_0^t \widetilde{G}(t,t')\vec{F}(t')dt', \quad (17)$$

where $G(t,t')$ is the Green function solution to the differential equation,

$$\widetilde{M}\frac{\partial^2\widetilde{G}}{\partial t^2} + \widetilde{\Gamma}\frac{\partial\widetilde{G}}{\partial t} + \widetilde{K}\widetilde{G} = \widetilde{1}\delta(t - t'). \quad (18)$$

Normally we need to specify the boundary conditions at $t = 0$. However, we are interested in the steady-state solution to the problem so the initial conditions are irrelevant. We can choose any initial condition that is convenient. In particular, we can choose $\vec{\chi}(0) = 0$ and $\dot{\vec{\chi}}(0) = 0$. With these conditions, the homogeneous term is zero, and our steady-state solution is

$$\vec{\chi}(t) = \int_0^t \widetilde{G}(t,t')\vec{F}(t')\,dt'. \quad (19)$$

We look for a solution to the Green function of the form,

$$\widetilde{G}(t,t') = (\widetilde{C}^{(1)}\widetilde{\chi}^{(1)}(t - t') + \widetilde{C}^{(2)}\widetilde{\chi}^{(2)}(t - t'))\eta(t - t'), \quad (20)$$

where $\widetilde{C}^{(1)}$ and $\widetilde{C}^{(2)}$ are matrices to be determined, $\eta(t - t')$ is the Heaviside step function, and

$$\widetilde{\chi}_{ij}^{(1)} = \left(\chi_i^{(1)}\right)_j \quad \text{and} \quad \widetilde{\chi}_{ij}^{(2)} = \left(\chi_i^{(2)}\right)_j, \quad (21)$$

particularly $(\chi_i^{(\alpha)})_j$ is the j^{th} component of the i^{th} solution $\chi_i^{(\alpha)}$ to the homogeneous equation of motion [Eq. (5)], and $\alpha\epsilon\{1,2\}$.

We introduce the operator $\widetilde{\Omega}$ such that

$$\widetilde{\Omega} = \widetilde{M}\frac{\partial^2}{\partial t^2} + \widetilde{\Gamma}\frac{\partial}{\partial t} + \widetilde{K}. \quad (22)$$

Equation (18) reduces to

$$\widetilde{\Omega}\widetilde{G} = \widetilde{1}\delta(t - t'), \quad (23)$$

inserting Eq. (20) in Eq. (23) produces

$$\begin{aligned}
&\widetilde{\Omega}G(t,t') \\
&= \eta(t-t')\widetilde{\Omega}[\widetilde{C}^{(1)}\widetilde{\chi}^{(1)}(t-t') + \widetilde{C}^{(2)}\widetilde{\chi}^{(2)}(t-t')] \\
&\quad + 2\widetilde{M}\frac{\partial}{\partial t}[\widetilde{C}^{(1)}\widetilde{\chi}^{(1)}(t-t') + \widetilde{C}^{(2)}\widetilde{\chi}^{(2)}(t-t')]\delta(t-t') \\
&\quad + \widetilde{M}[\widetilde{C}^{(1)}\widetilde{\chi}^{(1)}(t-t') + \widetilde{C}^{(2)}\widetilde{\chi}^{(2)}(t-t')]\delta'(t-t') \\
&\quad + \Gamma[\widetilde{C}^{(1)}\widetilde{\chi}^{(1)}(t-t') + \widetilde{C}^{(2)}\widetilde{\chi}^{(2)}(t-t')]\delta(t-t') \\
&= \widetilde{1}\delta(t-t'). \qquad (24)
\end{aligned}$$

At $(t-t'=0)$ we want this to equal the identity matrix $\widetilde{1}$. This will happen if

$$\begin{aligned}
&\widetilde{C}^{(1)}\widetilde{\chi}^{(1)}(0) + \widetilde{C}^{(2)}\widetilde{\chi}^{(2)}(0) = 0, \\
&(\widetilde{C}^{(1)}\widetilde{\chi}^{(1)}(0) + \widetilde{C}^{(2)}\widetilde{\chi}^{(2)}(0))_{ij} = \tfrac{1}{2}\delta_{ij}\widetilde{M}^{-1}_{ij}.
\end{aligned} \qquad (25)$$

This is a set of $2N^2$ variables $\widetilde{C}^{\alpha}_{ij}$ where $\alpha\epsilon\{1,2\}$ and $2N^2$ separate equations. This problem is solvable and the solution can be found numerically. Once these coefficients are found, the displacement of particles as a function of time can be constructed out of the solution in Eq. (19).

B. Thermal heat flux

In this section we develop an expression of the thermal heat flux as a function of the hot and cold bath temperatures using the steady-state solution to the displacements found in Sec. II A; Eq. (19). We will use the result derived in Appendix A; Eq. (A7) as an expression of the heat flux j_{ij} between particles i and j.

$$\begin{aligned}
aj_{ij} = &\frac{\partial V_{ij}}{\partial x_i}\dot{x}_i + \frac{\partial V_{ij}}{\partial y_i}\dot{y}_i + \frac{\partial V_{ij}}{\partial z_i}\dot{z}_i - \frac{\partial V_{ij}}{\partial x_j}\dot{x}_j \\
&- \frac{\partial V_{ij}}{\partial y_j}\dot{y}_j - \frac{\partial V_{ij}}{\partial z_j}\dot{z}_j,
\end{aligned} \qquad (26)$$

where

$$V_{ij} = (x_i,y_i,z_i)\begin{bmatrix} K_{3i-2,3j-2} & K_{3i-2,3j-1} & K_{3i-2,3j} \\ K_{3i-1,3j-2} & K_{3i-1,3j-1} & K_{3i-1,3j} \\ K_{3i,3j-2} & K_{3i,3j-1} & K_{3i,3j} \end{bmatrix}\begin{pmatrix} x_j \\ y_j \\ z_j \end{pmatrix}, \qquad (27)$$

and (x_i,y_i,z_i) and (x_j,y_j,z_j) are the components of the displacements of particles i and j, respectively. The K's are the elements of the K matrix involving the displacements of particles i and j.

$$\begin{aligned}
aj_{ij} = &K_{3i-2,3j-2}(x_j\dot{x}_i - x_i\dot{x}_j) + K_{3i-1,3j-1}(y_j\dot{y}_i - y_i\dot{y}_j) \\
&+ K_{3i,3j}(z_j\dot{z}_i - z_i\dot{z}_j) + K_{3i-2,3j-1}(y_j\dot{x}_i - x_i\dot{y}_j) \\
&+ K_{3i-1,3j-2}(x_j\dot{y}_i - y_i\dot{x}_j) + K_{3i-2,3j}(z_j\dot{x}_i - x_i\dot{z}_j) \\
&+ K_{3i,3j-2}(x_j\dot{z}_i - z_i\dot{x}_j) + K_{3i-1,3j}(z_j\dot{y}_i - y_i\dot{z}_j) \\
&+ K_{3i,3j-1}(y_j\dot{z}_i - z_i\dot{y}_j).
\end{aligned} \qquad (28)$$

Now that we have a working expression of the thermal heat flux j_{ij}, the next step is to replace the site displacement and velocities, by the steady-state solution Eq. (19) and its time derivative. In fact all the terms in parentheses in Eq. (28) are of the form $I_{ij} = (\dot{\vec{\chi}})_{3i-l}(\vec{\chi})_{3j-s} - (\dot{\vec{\chi}})_{3j-s}(\vec{\chi})_{3i-l}$, where (s,l) are integers between 1 and 3, which is also expressed as

$$\begin{aligned}
I_{3i-l,3j-s} = &\sum_{mn}, \int_0^t dt_1 \int_0^t dt_2 \widetilde{G}_{3i-l,m}(t-t_1)\widetilde{G}_{3j-s,n}(t-t_2) \\
&\times F_m(t_1)F_n(t_2) - \int_0^t dt_1 \int_0^t dt_2 \widetilde{G}_{3i-l,m}(t-t_1) \\
&\times \widetilde{\widetilde{G}}_{3j-s,n}(t-t_2)F_m(t_1)F_n(t_2),
\end{aligned} \qquad (29)$$

using Eq. (4), and noting that we are only applying a driving force to the first and last particles. Equation (29) reduces to

$$\begin{aligned}
I_{3i-l,3j-s} = &2\gamma_N kT_N \sum_{n=1}^{3}\int_0^t dt_1 \widetilde{G}_{3i-l,3N-n}(t-t_1) \\
&\times \widetilde{\widetilde{G}}_{3j-s,3N-n}(t-t_1) - 2\gamma_1 kT_1 \sum_{m=1}^{3}\int_0^t dt_1 \widetilde{G}_{3i-l,m} \\
&\times (t-t_1)\widetilde{\widetilde{G}}_{3j-s,m}(t-t_1),
\end{aligned} \qquad (30)$$

and Eq. (28) becomes

$$j_{ij} = \sum_{l=1}^{3}\sum_{s=1}^{3}\frac{K_{3i-l,3j-s}}{a} I_{3i-l,3j-s}. \qquad (31)$$

Let S_{ij} and S'_{ij} be the coefficients of T_1 and T_N in Eq. (30),

$$\begin{aligned}
S'_{ij} &= 2\gamma_N k \sum_{n=1}^{3}\int_0^t dt_1 \widetilde{G}_{i3N-n}(t-t_1)\widetilde{\widetilde{G}}_{j3N-n}(t-t_1), \\
S_{ij} &= 2\gamma_1 k \sum_{m=1}^{3}\int_0^t dt_1 \widetilde{G}_{im}(t-t_1)\widetilde{\widetilde{G}}_{jm}(t-t_1).
\end{aligned} \qquad (32)$$

Equation (31) reduces to

$$\begin{aligned}
j_{ij} = &T_N \sum_{l=1}^{3}\sum_{s=1}^{3}\frac{K_{3i-l,3j-s}}{a} S'_{3i-l,3j-s} \\
&- T_1 \sum_{l=1}^{3}\sum_{s=1}^{3}\frac{K_{3i-l,3j-s}}{a} S_{3i-l,3j-s}.
\end{aligned} \qquad (33)$$

The coefficients of T_1 and T_N in Eq. (33) can be calculated numerically using the expression of the Green functions found in Sec. II A; Eq. (20). In principle we can apply the Langevin driving force to any of the atoms in the system. In order to estimate the thermal conductivity we choose to couple to atoms at the furthest extremes of the chain. The rationale is that they are furthest from the stiffer incorporated molecule and thus best connected to the fluctuating heat bath.

The localized heat flux j_i is the sum of all the individual contributions from the sites j nearest to i:

$$j_i = \sum_j j_{ij}. \qquad (34)$$

The total heat flux is the sum of the localized contribution,

$$j = \sum_i j_i = \sum_{ij} j_{ij} = D_h T_N - D_c T_1, \qquad (35)$$

where

$$D_h = \sum_{ij}\sum_{sl=1}^{3} \frac{K_{3i-l,3j-s}}{a} S'_{3i-l,3j-s},$$
$$D_c = \sum_{ij}\sum_{sl=1}^{3} \frac{K_{3i-l,3j-s}}{a} S_{3i-l,3j-s}. \quad (36)$$

We will numerically show in Sec. III that the total heat flux j in Eq. (35) is proportional to the temperature difference of the hot and cold baths (i.e., $D_h = D_c$).

C. Participation ratio

In order to better understand how to optimize structures we find it useful to calculate the participation ratio (P) [19]. This quantity is commonly used in electronic problems to describe the degree to which an electron is localized in space [20]. The participation ratio is defined as

$$P = \frac{\left(\sum_{n=1}^{n=N} {\psi_n}^2\right)^2}{L^d \sum_{n=1}^{n=N} {\psi_n}^4}, \quad (37)$$

where N is the total number of modes, $|\psi\rangle$ is the eigenvector describing the normal mode, L the system linear size, and d is the Euclidean dimension of the system, giving the total number of atoms $L^d = N$.

The participation ratio is in the order of 1 for extended modes and $\approx 1/N$ for localized modes. The intuition is that systems with more low-energy, high-participation ratio modes will be better at conducting heat.

III. APPLICATION

In this section we shall present the application of the results of Sec. II for two special cases, a one-dimensional linear chain and a small two-dimensional functionalized sheet of graphene.

A. One-dimensional chain

Consider a linear chain of N coupled atoms, the first and the last of which interact with thermal heat baths. The schematic diagram of this setup is drawn in Fig. 1 for $N = 4$. For simplicity only nearest neighbor interactions will be considered and it is assumed that adjacent atoms are coupled with springs of spring constant K. Let x_l be the displacement of the l^{th} particle. The Hamiltonian of this system is

$$H = \sum_i \frac{{p_i}^2}{2m} + \frac{1}{2}K(x_{i+1} - x_i)^2, \quad (38)$$

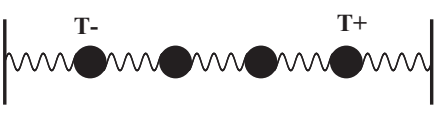

FIG. 1. A pictorial representation of a linear chain of $N = 4$ mutually coupled oscillators in interaction with two thermal reservoirs working at different temperatures. Here $T_1 = T_+$ and $T_N = T_-$.

where m is the mass of the particles. We set $m = a = 1$, where a is the lattice constant, and $K = 1$.

In this one-dimensional case Eqs. (26) and (30) reduce to

$$j_{ij} = \left(\frac{K}{a}\right)(x_j\dot{x}_i - x_i\dot{x}_j) = \left(\frac{K}{a}\right) I_{ij}, \quad (39)$$

where

$$I_{ij} = 2\gamma_N kT_N \int_0^t dt_1 \widetilde{G}_{iN}(t-t_1)\widetilde{\widetilde{G}}_{jN}(t-t_1) - 2\gamma_1 kT_1 \int_0^t dt_1 \widetilde{G}_{i1}(t-t_1)\widetilde{\widetilde{G}}_{j1}(t-t_1). \quad (40)$$

The total heat flux is

$$j = \sum_{ij} j_{ij} = \left(\frac{K}{a}\right)\sum_{ij} I_{ij} = D_h T_N - D_c T_1, \quad (41)$$

where

$$D_h = 2\gamma_N k\left(\frac{K}{a}\right)\sum_{ij}\int_0^t dt_1 \widetilde{G}_{iN}(t-t_1)\widetilde{\widetilde{G}}_{jN}(t-t_1),$$
$$Dc = 2\gamma_1 k\left(\frac{K}{a}\right)\sum_{ij}\int_0^t dt_1 \widetilde{G}_{i1}(t-t_1)\widetilde{\widetilde{G}}_{j1}(t-t_1). \quad (42)$$

Figure 2 is a plot of the coefficients of T_N and T_1 in Eq. (41) as a function of time for a chain of four atoms. As illustrated, these coefficients converge to the same value. This means that in the steady-state regime the total heat flux j is proportional to the temperature difference of the hot and cold baths, the proportionality constant is the thermal conductance of the chain λ_c, and

$$j = \lambda_c(T_N - T_1). \quad (43)$$

B. Two-dimensional sheet of graphene

In this application we consider a hexagonal sheet of graphene made of 36 carbon atoms bonded together in a honeycomb structure. We attach two alkane chains to opposite

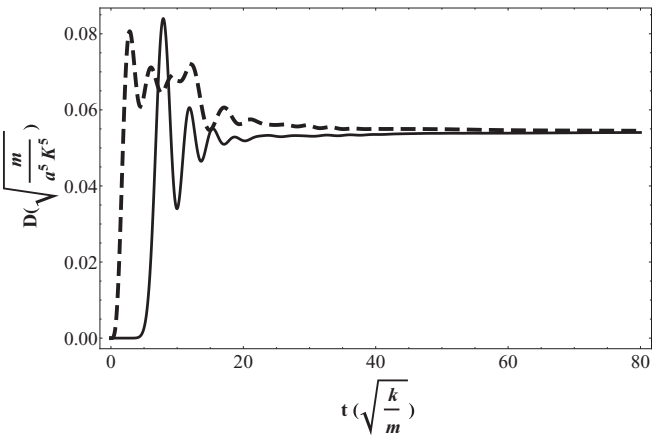

FIG. 2. ($D_h = \frac{K}{a}\sum_{ij} S'_{ij}$) and ($D_c = \frac{K}{a}\sum_{ij} S_{ij}$) as a function of time (t) for a chain of four atoms. As expected these factors converge to the same value. This means that in the steady-state regime the total heat flux j is proportional to the temperature difference of the hot and cold baths.

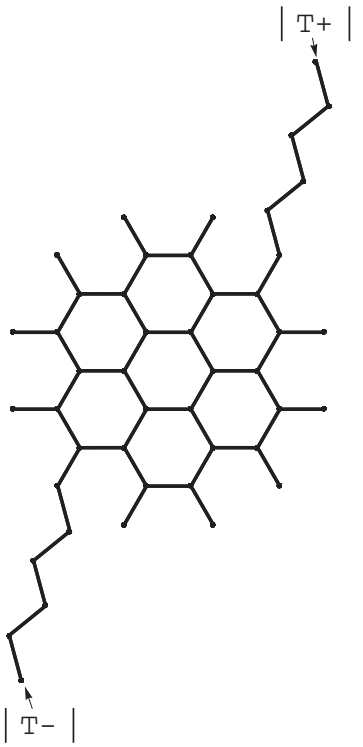

FIG. 3. A pictorial representation of a functionalized sheet of graphene. The number of atoms in the graphene sheet is 36. The alkane chains are n-pentane. The end of the chains interact with two thermal reservoirs working at different temperatures.

boundaries of the graphene sheet and to the heat baths as shown in Fig. 3. The alkane chains are n-pentane. The Tersoff-Berner (TB) force field is used to describe the interactions among the atoms in the graphene sheet. The Nath, Escobedo, and Pablo revised (NERD) potential is used to describe the interactions in the chains and the bond between the chains and the graphene.

We relax the system by minimizing the site potential in the functionalized graphene sheet; this is done by using a multiobjective optimization technique [22]. Additional information about the (TB) and (NERD) force fields is found in Appendix B.

The next step to solving the problem of heat conduction in the functionalized graphene is to find the normal modes of the structure. At this point we assume that the site displacements are very small and approximate the potential (E) by a second-order Taylor expansion around the site equilibrium positions,

$$E = \frac{1}{2}\sum_{ij}\frac{\partial^2 V}{\partial\zeta_i\partial\zeta_j}\zeta_i\zeta_j. \tag{44}$$

The second derivatives of the potential energy are the elements of the $\widetilde{K}$ matrix that was introduced in Sec. II,

$$\widetilde{K}_{ij} = \frac{\partial^2 V}{\partial\zeta_i\partial\zeta_j}. \tag{45}$$

We then proceed as described in Sec. II and solve for the Green function and the particle displacement in the stationary regime. We numerically calculate the heat flux from Eqs. (26), (30), (34), and (35) as a function of the hot and cold bath temperatures.

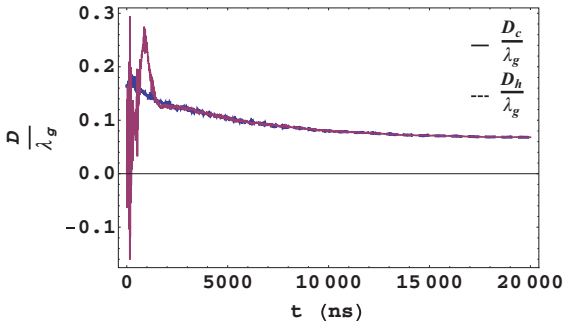

FIG. 4. (Color online) (a) Time evolution (D_h/λ_g) and (D_c/λ_g). As expected (D_h/λ_g) and (D_c/λ_g) converge to the same value. This means that in the steady-state regime the total heat flux is proportional to the temperature difference of the hot and cold baths.

1. *Numerical results of thermal heat flux in functionalized graphene*

The total heat flux in the functionalized graphene sheet was numerically calculated. Figure 4 represents the time evolution of the ratio of the hot and cold temperature coefficients (D_h) and (D_c) in Eq. (35) and the thermal conductance of the graphene (λ_g) calculated using the same technique by taking the chains off the graphene and attaching two opposite sites to hot and cold baths. As expected, in the steady-state regime these factors converge to the same value. This confirms as in the previous case of linear chains that the heat flux is proportional to the temperature difference of the hot and cold baths. The proportionality constant is the thermal conductance of the functionalized grapehene.

2. *Effect of changing the length of the chains on the thermal conduction*

In this section we shall use the technique just developed to investigate the effect of changing the length of the chains on the thermal conduction of heat throughout the functionalized graphene. Figure 5 summarizes the results of thermal conductance for chain lengths between $N = 3$ and $N = 11$. In each case we connect two identical chains on opposite sides of the boundaries to the graphene sheet. The opposite ends of each chain are connected to two heat baths at temperatures

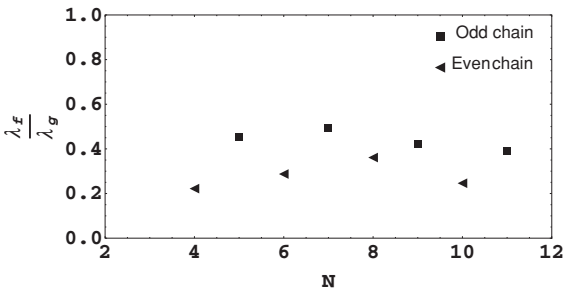

FIG. 5. The ratio of the thermal conductance of functionalized graphene λ_f to the thermal conductance of graphene λ_g as a function of chain length.

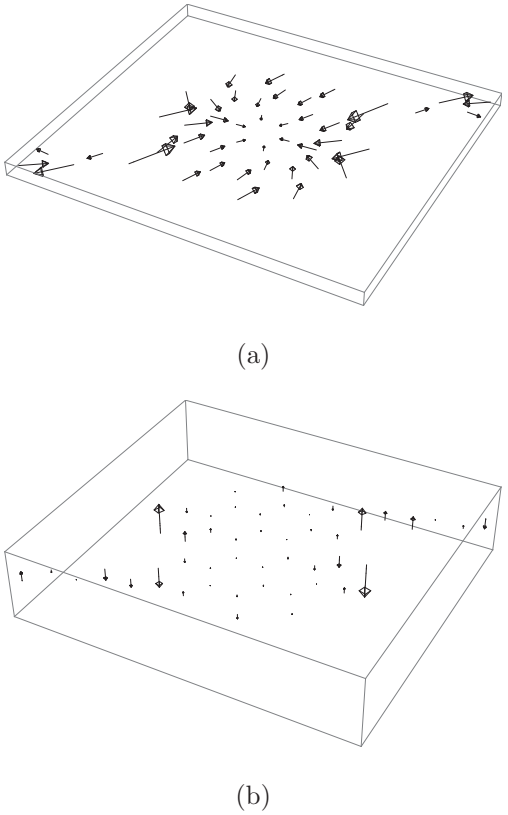

FIG. 6. Pictorial representation of a high-participation ratio mode ($P = 0.86$) (a), and a low-participation ratio mode ($P = 0.13$).

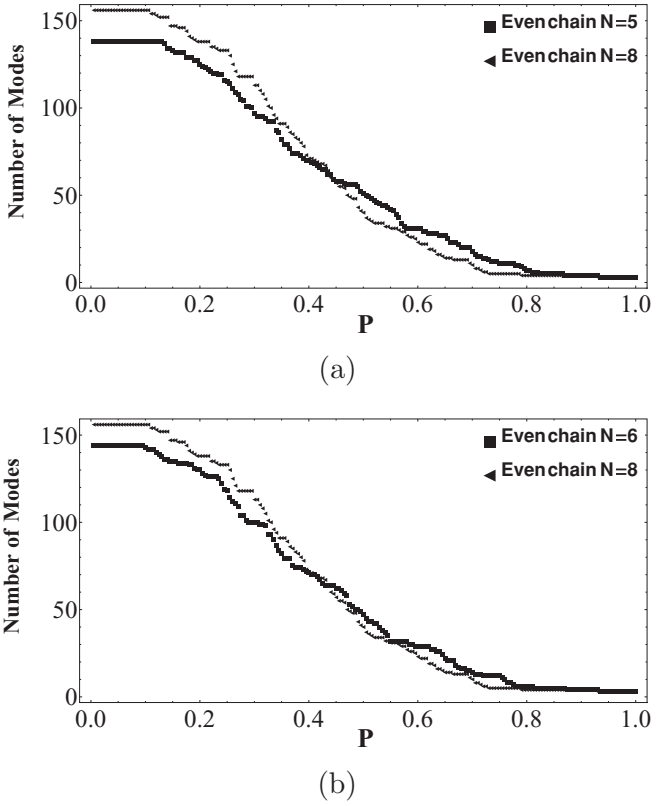

FIG. 7. (Color online) Number of modes with increasing participation ratios for functionalized graphene configurations with five, six, and eight chain sites.

$T+$ and $T-$. Based on these results, functionalized graphene with odd alkane chains perform better in terms of thermal conductance than with even alkane chains. For each type of chains, the thermal conductance increases with the chain length for smaller alkane chains but then decreases with longer chains.

To understand the underlying causes of this result, we calculated the participation ratio (P) for each normal mode in each configuration. The extended modes, the main contributor to the heat transport, can be identified by their higher participation ratios. In contrast, low-participation ratio modes contribute less to the heat transport. Figure 6 is a pictorial representation of the site displacements of a high- and low-participation ratio mode for the structure in Fig. 3; notice the larger magnitude of the site displacement, and the extent of the mode with larger participation ratio. Figure 7 represents the total number of modes with increasing participation ratio for configurations similar to the structure in Fig. 3 with five, six, and eight chain sites ($N = 5,6,8$); notice that the number of extended modes with high-participation ratios decreases with the increase in the size of the chains. This is fairly noticeable for longer chains, and in fact explains the longer chains' smaller thermal conductance. Particularly for even and odd chains as shown in Fig. 7(a) this pattern also includes some of the low-participation ratio modes. Odd chains perform better than even chains in conducting heat because of their larger number of moderate- and high-participation ratio modes contributing to the heat transport.

3. *Effect of the noise*

Our approach is entirely classical. This is, in part, by design, since we produce systems of equations that are rapidly and easily soluble. However, the Langevin equation is well known to produce equipartition [18]. This means that all modes, even those with extremely high frequency, will have a nonzero occupation. This probably results in an overestimate of the thermal conductivity since some high-participation modes may have too high an energy to have any occupation at room temperature. Mathematically, this arises from the assumption of a delta-function correlation in time for the driving forces, since all frequencies must be included to have zero correlation time. Possible solutions include using a more complicated set of driving forces that are explicitly quantum mechanical [22], and inserting a fictitious correlation time into the driving force (Ornstein-Uhlenbeck noise) that is itself chosen to be temperature dependent to mimic the effect of a Bose-Einstein suppression of high-energy modes [23].

IV. CONCLUSION

Improving heat transport in functionalized graphene is important to a large number of systems. In this paper we have demonstrated an efficient and straightforward method for calculating the thermal heat flux. The results of this simulation can be used to design and test different configurations and to find the one that conveys the largest amount of heat. As an application of this method, we investigated the effect of changing the length of the chains on the overall thermal

conduction. The numerical results showed that odd alkane chains perform better than even alkane chains. In addition, very long alkane chains deteriorate the overall heat transport. This can be seen as the limit of simply embedding the stiff material in a very soft, infinite matrix.

There are many ways this approach can be expanded. For ease of application we chose to only drive the outermost ends of the functionalized chains. This can easily be expanded to include driving many or all of the atoms in the system. However, the Langevin approach assumes complete incoherence between all the driving forces. This will not be true on an atomic level since the local phonon environment will have some nonzero coherence length. The physical details of the local environment and its coherence are interesting in their own right, but should not profoundly change results found in this approach: Systems in which the external chains are well-coupled to the main structure will still have superior thermal conductivity to those that do not.

APPENDIX A: FLUX

The goal of this section is to give a definition of the heat flux in terms of quantities we can calculate. The heat flux $\vec{j}(\vec{r},t)$ at time t in the spatial position $\vec{r}$ is nothing but the energy current, implicitly defined by the continuity equation,

$$\frac{dh(\vec{r},t)}{dt} + \vec{\nabla}\cdot\vec{j} = 0, \tag{A1}$$

where $h(\vec{r},t)$ is the energy density.

With reference to an ensemble of interacting particles, we can write the microscopic energy density as the sum of the isolated contributions located in the instantaneous position of each particle.

$$h(\vec{r},t) = \sum_i h_i \delta(\vec{r} - \vec{r}_i), \tag{A2}$$

where $\delta(\vec{r})$ is the Dirac distribution and

$$h_i(\vec{r},t) = \frac{p_i^2}{2m_i} + \frac{1}{2}\sum_{j\neq i} V_{ij} \tag{A3}$$

is the energy contribution of the i^{th} particle. The first term correspond to the kinetic energy. The last term amounts to half of the potential energy of the pairwise interactions with the neighboring particles. In a similar way we can write the heat flux as the sum of the localized contributions,

$$\vec{j}(\vec{r},t) = \sum_i \vec{j}_i \delta(\vec{r} - \vec{r}_i), \tag{A4}$$

the problem amounts therefore to give a definition of the local heat flux $j_i(\vec{r},t)$.

In the limit of small oscillations around the equilibrium position, density fluctuation can be neglected and $h_i(\vec{r},t)$ is proportional to the energy density.

The time derivative of $h_i(\vec{r},t)$ is

$$\begin{aligned}\frac{dh_i(\vec{r},t)}{dt} = &-\frac{1}{2}\sum_{j\neq i}\left(\frac{\partial V_{ij}}{\partial x_i}\dot{x}_i + \frac{\partial V_{ij}}{\partial y_i}\dot{y}_i + \frac{\partial V_{ij}}{\partial z_i}\dot{z}_i\right)\\ &+\frac{1}{2}\sum_{j\neq i}\left(\frac{\partial V_{ij}}{\partial x_j}\dot{x}_j + \frac{\partial V_{ij}}{\partial y_j}\dot{y}_j + \frac{\partial V_{ij}}{\partial z_j}\dot{z}_j\right).\end{aligned} \tag{A5}$$

This equation can in turn be written as

$$\frac{dh_i}{dt} = -\sum_j \frac{j_{ij}}{a}, \tag{A6}$$

where a is the distance to the nearest neighbor. The local heat flux j_{ij} is such that

$$\begin{aligned}a j_{ij} = &\frac{\partial V_{ij}}{\partial x_i}\dot{x}_i + \frac{\partial V_{ij}}{\partial y_i}\dot{y}_i + \frac{\partial V_{ij}}{\partial z_i}\dot{z}_i - \frac{\partial V_{ij}}{\partial x_j}\dot{x}_j\\ &- \frac{\partial V_{ij}}{\partial y_j}\dot{y}_j - \frac{\partial V_{ij}}{\partial z_j}\dot{z}_j.\end{aligned} \tag{A7}$$

The total heat flux j is the sum of all the isolated contributions located in the instantaneous positions of each particle in the system,

$$j = \sum_{ij} j_{ij}. \tag{A8}$$

APPENDIX B: EXPLICIT FORM OF THE POTENTIALS

1. The Tersoff-Brenner potential

The Tersoff-brenner (TB) potential was employed to describe the interactions among the atoms in the graphene sheet. In the TB force field, the potential energy is modeled as a sum of pairlike interactions, where the coefficient of the attractive term in the pairlike potential depends on the local environment, yielding an effective many-body potential.

The interatomic potential is taken to have the form,

$$\begin{aligned}E = \sum_i E_i = \frac{1}{2}\sum_{i\neq j} V ij,\\ V_{ij} = f_c(r_{ij})[f_R(r_{ij}) + b_{ij} f_A(r_{ij})].\end{aligned} \tag{B1}$$

Here E is the total energy of the system, which is decomposed into a site energy E_i and a bond energy V_{ij}. The indices i and j run over the atoms of the system, and r_{ij} is the distance from atom i to atom j.

The function f_R represents a repulsive pair potential which includes the orthogonalization energy when atomic wave functions overlap, and f_A represents an attractive pair potential associated with bonding. The extra term f_c is merely a smooth cutoff function, to limit the range of the potential, since for many applications like the one we are running short-ranged functions permit a tremendous reduction in computational effort.

The function b_{ij} represents a measure of the bond order. All these functions are taken to be of the following form:

$$\begin{aligned}f_R(r_{ij}) &= A\exp(-\lambda r_{ij}),\\ f_A(r_{ij}) &= B\exp(-\mu r_{ij}),\\ b_{ij} &= \left(1+\beta^n \zeta_{ij}^n\right)^{-1/2n},\\ \zeta_{ij} &= \sum_{k\neq i,j} f_c(r_{ij}) g(\theta_{ijk}) \exp\left[\lambda_3^3 (r_{ij} - r_{ik})^3\right],\\ g(\theta) &= 1 + \frac{c^2}{d^2} - \frac{c^2}{[d^2 + (h - \cos(\theta))^2]},\end{aligned} \tag{B2}$$

TABLE I. TB parameters for carbon.

TB parameters for carbon	
A (eV)	1.3936×10^3
B (eV)	3.467×10^2
λ (Å^{-1})	3.4879
μ (Å^{-1})	2.2119
β	1.5724×10^{-7}
n	7.2751×10^{-1}
c	3.8049×10^4
d	4.384×10^0
h	-5.7058×10^{-1}
R (Å)	1.95
S (Å)	0.15

TABLE II. Intramolecular potential energy parameters.

Bond stretching potential	b_{eq}(Å)	k_r/k_B (K/Å^2)		
$CH_x - CH_y$	1.54	96 500		
Bond bending potential				
	$\theta_0(^o)$	k_θ/k_B (K)		
$CH_x - (CH_2) - CH_y$	114.0	625 00		
$CH_x - (CH) - CH_y$	109.47	62 500		
$CH_x - (C) - CH_y$	109.47	62 500		
Torsional potential				
(K)	V_o/k_B	V_1/k_B	V_2/k_B	V_3/k_B
$C - C - C - C$	0	355.04	−68.19	791.32

where θ_{ijk} is the bond angle between bond ij and ik. The cutoff function is taken to be a step-down function so to include only the first and next nearest neighbors to each site.

Parameters and more details necessary to implement the TB force field are listed in Table I.

2. The NERD potential

A united atom representation of the alkanes is adopted throughout this work. The alkanes considered were n-pentane, n-heptane, and n-nonane. Within the united atom description, an n-alkane molecule is described as a flexible linear chain of methylene (CH_2) pseudoatoms terminating at both ends with methyl (CH_3) pseudoatoms. The parameters were taken from the NERD force field [24,25]. In this simulation we ignore the potential due to interactions between sites, which are separated by more than three bonds as well as interactions between sites that belong to different molecules. A complete listing of all of the intermolecular potential parameters for saturated alkanes in the NERD force field is given in Table II.

The potential in the branched alkane chains is divided between bond stretching potential U_r, bond bending potential U_θ and a torsional potential U_ϕ where

$$\begin{aligned} U_r &= \tfrac{1}{2}k_r(r - r_o)^2, \\ U_\theta &= \tfrac{1}{2}k_\theta(\theta - \theta_o)^2, \end{aligned} \tag{B3}$$

and r_o and θ_o denote the equilibrium bond length and bond angle, respectively.

$$\begin{aligned} U_\phi = V_o + V_1[1 + \cos(\phi)] + V_2[1 - \cos(2\phi)] \\ + V_3[1 + \cos(3\phi)]. \end{aligned} \tag{B4}$$

[1] J. Che, T. Cagin, and W. A. Goddard, Nanotechnology **11**, 65 (2000).
[2] J. Home, B. Batlogg, Z. Benes, A. T. Johnson, and J. E. Fisher, Science **289**, 1730 (2000).
[3] S. Berber, Y. K. Kwon, and D. Tomanek, Phys. Rev. Lett. **84**, 4613 (2000).
[4] S. V. Morozov, K. S. Novoselov, M. I. Katsnelson, F. Schedin, D. C. Elias, J. A. Jaszczak, and A. K. Geim, Phys. Rev. Lett. **100**, 016602 (2008); S. V. Morozov, K. S. Novoselov, and A. K. Geim, Phys. Usp. **51**, 744 (2008).
[5] K. I. Bolotin, K. J. Sikes, Z. Jiang, M. Klima, G. Fudenberg, J. Hone, P. Kim, and H. L. Stormer, Solid State Commun. **146**, 351 (2008).
[6] A. A. Balandin, S. Ghosh, W. Bao, I. Calizo, D. Teweldebrhan, F. Miao, and C. N. Lau, Nano Lett. **8**, 902 (2008).
[7] D. L. Nika *et al.*, Appl. Phys. Lett. **94**, 203103 (2009).
[8] S. Ghosh *et al.*, Nat. Mater. **9**, 555 (2010).
[9] L. Li and D. D. L. Chung, J. Electron. Mater. **23**, 557 (1994).
[10] K. C. Yung and H. Liem, J. Appl. Polym. Sci. **106**, 3587 (2007).
[11] M. J. Biercuk, M. C. Llahuno, M. Radosavljevic, J. K. Hyun, and A. T. Jonson, Appl. Phys. Lett. **80**, 2767 (2002).
[12] S. Ghosh, I. Calizo, D. Teweldebrhan, E. P. Pokatilov, D. L. Nika, A. A. Balandin, W. Bao, F. Miao, and C. N. Lau, Appl. Phys. Lett. **92**, 151911 (2008).
[13] P. L. Kapitza, Zh. Eksp. Teor. Fiz. **11**, 1 (1941) [J. Phys. (USSR) **4**, 181 (1941)]; in *Collected Papers of P. L. Kapitza*, edited by D. ter Haar, Vol. 2 (Pergamon, Oxford, 1965), p. 581.
[14] P. L. Kapitza, Zh. Eksp. Teor. Fiz. **11**, 1 (1941).
[15] K. Wakabayashi, M. Fujita, H. Ajiki, and M. Sigrist, Phys. Rev. B **59**, 8271 (1999).
[16] M. C. Lemme, T. J. Echtermeyer, M. Baus, and H. Kurz, IEEE Electron Device Lett. **28**, 282 (2007).
[17] X. Li, X. Wang, Li Zhang, S. Lee, and H. Dai, Science **319**, 1229 (2008).
[18] H. Risken and T. Frank, *The Fokker-Planck Equation: Methods of Solutions and Applications* (Springer Series in Synergetics, New York, 1996).
[19] M. Zheng, M. Goda, K. Yakubo, and K. W. Yu, J. Phys. Soc. Jpn. **77**, 094601 (2008).
[20] A. P. Korte and G. H. M. van der Heijden, J. Phys. Condens. Matter **21**, 495301 (2009).
[21] R. E. Steuer, *Multiple Criteria Optimization: Theory, Computations, and Application* (John Wiley & Sons, New York, 1986).
[22] S. Attal and A. Joye, J. Funct. Anal. **247**, 253 (2007).
[23] A. A. Moussa and K. Mullen (unpublished).
[24] F. A. Escobedo and J. J. de Pablo, J. Chem. Phys. **105**, 4391 (1996).
[25] S. K. Nath and J. J. de Pablo, Mol. Phys. **98**, 231 (2000).